Article No. jmbi.1999.3027 available online at http://www.idealibrary.com on IDEAL® J. Mol. Biol. (1999) 291, 899–911

JMB

Structure of Bacteriorhodopsin at 1.55 Å Resolution

Hartmut Luecke[1,2]*, Brigitte Schobert[2], Hans-Thomas Richter[2] Jean-Philippe Cartailler[1] and Janos K. Lanyi[2]*

[1]*Department of Molecular Biology and Biochemistry University of California, Irvine CA, 92697, USA*

[2]*Department of Physiology and Biophysics, University of California, Irvine, CA 92697, USA*

**Corresponding authors*

The atomic structure of the light-driven ion pump bacteriorhodopsin and the surrounding lipid matrix was determined by X-ray diffraction of crystals grown in cubic lipid phase. In the extracellular region, an extensive three-dimensional hydrogen-bonded network of protein residues and seven water molecules leads from the buried retinal Schiff base and the proton acceptor Asp85 to the membrane surface. Near Lys216 where the retinal binds, transmembrane helix G contains a π-bulge that causes a non-proline? kink. The bulge is stabilized by hydrogen-bonding of the main-chain carbonyl groups of Ala215 and Lys216 with two buried water molecules located between the Schiff base and the proton donor Asp96 in the cytoplasmic region. The results indicate extensive involvement of bound water molecules in both the structure and the function of this seven-helical membrane protein. A bilayer of 18 tightly bound lipid chains forms an annulus around the protein in the crystal. Contacts between the trimers in the membrane plane are mediated almost exclusively by lipids.

© 1999 Academic Press

Keywords: bacteriorhodopsin; membrane proteins; proton pump; hydrogen-bonded chain; X-ray crystallography

Introduction

Recent progress in determining the structures of crystallized membrane proteins has focused renewed attention on how ions are transported across biological membranes and on how receptors transmit transmembrane signals. The resolutions for these proteins are greatly improved (e.g. see Iwata *et al*., 1995, 1998; Tsukihara *et al*., 1996; Xia *et al*., 1997), but have not approached those of the truly atomic resolution models obtained from crystals of soluble proteins. The structure of bacteriorhodopsin (reviewed most recently by Lanyi, 1997; Oesterhelt, 1998) is now described at 1.55 Å resolution. Bacteriorhodopsin is the best understood ion pump, a homologue of sensory rhodopsins (Hoff *et al*., 1997), and the structural prototype of G protein-coupled receptors and other proteins that contain transmembrane helices. It is a small (26 kDa) protein of seven transmembrane helices and short interhelical loops and extramembrane N and C termini. In the last few years its atomic structure has been determined at various resolutions between 3.5 and 2.3 Å (Grigorieff *et al*., 1996; Kimura *et al*., 1997; Pebay-Peyroula *et al*., 1997; Luecke *et al*., 1998; Essen *et al*., 1998; Takeda *et al*., 1998; Mitsuoka *et al*., 1999). This light-driven ion pump is energized by photoisomerization of the all-*trans* retinal chromophore to 13-*cis*. In the 2.3 Å resolution structure (Luecke *et al*., 1998), the arrangement of a hydrogen-bonded network of protein residues and water molecules between the centrally located retinal Schiff base and the extracellular surface, together with earlier spectroscopic and mutational evidence, suggested how a proton could be translocated through this region. The structure of the unphotolyzed state revealed less about the path of the transported proton between the cytoplasmic surface and the retinal, but indirect evidence (Cao *et al*., 1991; Sass *et al*., 1997; Kamikubo *et al*., 1997) had pointed to the involvement of water molecules in the large-scale protein conformational change in the cytoplasmic region (Dencher *et al*., 1989; Subramaniam *et al*., 1993; Han *et al*., 1994; Brown *et al*., 1995; Váró *et al*., 1996; Thorgeirsson *et al*., 1997).

The bacteriorhodopsin structure and the large-scale conformational change during the photocycle are likely to be directly relevant to the homologous sensory rhodopsins I and II, which function as phototaxis receptors in *Halobacterium*

E-mail address of the corresponding authors: hudel@uci.edu; jlanyi@orion.oac.uci.edu

0022-2836/99/340899–13 $30.00/0

© 1999 Academic Press

Table 1. X-ray data collection and refinement statistics

Data reduction resolution range (Å)	1.55-25.0	1.55-1.58	1.95-2.02
Total observations	372,549		
Unique structure factors	34,002		
R_{merge} (%)[a]	6.9	38.1	9.0
Average $I/\sigma(I)$[b]	19.9	2.0	8.7
Completeness (%)	99.1	97.2	99.4
Mosaicity (°)	0.61		
Refinement resolution range (Å)	1.55-12.0		
Number of structure factors	32,249		
Number of restraints	8209		
Number of parameters	8300		
Twin ratio	76:24		
Number of protein atoms	1721		
Number of retinal atoms	20		
Number of water molecules	24		
Number of lipid atoms	310		
R-factor (%) for data with $F > 4\ \sigma(F)$/all data[c]	14.0/15.8		
R_{free} (%) for data with $F > 4\ \sigma(F)$/all data[d]	20.1/22.5		
Average protein B (Å^2)	26.2		
Average retinal B (Å^2)	18.2		
Average water B (Å^2)	32.9		
Average lipid B (Å^2)	56.6		
Deviation from ideal bond lengths (Å)	0.010		
Deviation from ideal bond angle (°)	0.030		

[a] $R_{merge}\ (I) = \Sigma_{hkl}\ \Sigma_i \mid I_{hkl,i} - \langle I_{hkl}\rangle \mid / \Sigma_{hkl}\ \Sigma_i \mid I_{hkl,i}\mid$, where $\langle I_{hkl}\rangle$ is the average intensity of the multiple $I_{hkl,i}$ observations for symmetry-related reflections.

[b] $I/\sigma(I)$, average of the diffraction intensities, divided by their standard deviations.

[c] R-factor $= \Sigma_{hkl} \mid F_o - F_c \mid / \Sigma_{hkl} \mid F_o \mid$, where F_o and F_c are observed and calculated structure factors, respectively.

[d] $R_{free} = \Sigma_{hkl\ \varepsilon T} \mid F_o - F_c \mid / \Sigma_{hkl\varepsilon T}\ \mid F_o \mid$, where the test set (5% of the data) is omitted from the refinement in such a way that all structure factors in each of several thin resolution shells were selected to avoid bias due to the presence of merohedral twinning.

salinarum. In particular, sensory rhodopsin I was shown to function as a light-driven proton pump in the absence of its transducer protein (Spudich, 1994), and mutant evidence indicates that a conformational change, analogous to that in bacteriorhodopsin and coupled to the transmembrane helices of the transducer, mediates the signal transduction (Spudich *et al*., 1997; Zhang *et al*., 1999).

We report here on the structure of the unphotolyzed protein at a resolution (Table 1) that unambiguously identifies the configuration of the retinal and its binding site, specifies all intramembrane residue and backbone interactions and many in the interhelical loops, locates all hydrogen-bonded water molecules in the protein interior, and describes the arrangement of lipids in the bilayer.

Results and Discussion

The overall structure

The helical peptide backbone traverses seven times across the width of the membrane, as described in the initial reports at $\geqslant$3.5 Å resolution (Henderson *et al*., 1990; Grigorieff *et al*., 1996). The more recent structures with increasing resolution converge on a model in which the largest differences from the earlier models are in the loop regions and in the arrangement of the side-chains (RMS of positions for side-chain atoms >3 Å), but significant differences exist also in the main chain (Table 2). The B-C interhelical loop forms a twisted anti-parallel β-sheet on the extracellular surface, stabilized by six hydrogen bonds. Bacteriorhodopsin monomers form a very tight trimeric unit that is stabilized by extensive helix-helix contacts that bury 15,942 Å^2 (26.8% of each monomer surface), and include an intermolecular salt-bridge between Lys40 and Asp104 (Essen *et al*., 1998).

The retinal lies transversely in the intramembrane cavity formed by the seven transmembrane helices. As shown in Table 3, there are between one and five side-chain to main-chain or side-chain to side-chain hydrogen bonds between each pair of neighboring helices. These will ensure their close proximity, as required for the barrel-like structure. There are 19 such hydrogen bonds. Side-chain to side-chain hydrogen bonds between non-adjoining helices, which will contribute additionally to the stability of the tertiary structure, number 12 (Table 3). It may be because of these extensive interhelical interactions (a total of 31 hydrogen bonds) that the tertiary structure of the monomer does not depend on the trimeric arrangement in the rigid lattice of the purple membrane, and that the monomer can transport protons (Dencher & Heyn, 1979). Many of the interhelical hydrogen bonds are between residues that participate in proton transfers (see below), and these may be expected to have roles in stabilizing the structure and in the changes in the structure during the photocycle.

Table 2. Comparison of 1C3W with earlier atomic bacteriorhodopsin structures

PDB code (reference)	Main-chain RMS (Å)	Side-chain RMS (Å)	All-atom RMS (Å)	Resolution (Å)	Method
2BRD (1)	1.71	3.21	2.57	3.5	EM
1AP9 (2)	1.58	3.22	2.54	2.35	X-RAY, CLP
1AT9 (3)	0.82	1.67	1.33	3.0	EM
2AT9 (4)	1.08	1.55	1.36	3.0	EM
1BM1 (5)	0.70	2.03	1.52	3.5	X-RAY, detergent
1BRX (6)	0.35	1.10	0.82	2.3	X-RAY, CLP
1BRR[a] (7)	0.47	1.18	0.90	2.9	X-RAY, detergent

Residues 7-152 and 167-225 of the previously published bacteriorhodopsin structures were aligned with 1C3W (1.55 Å), using the program Swiss-PdbViewer (Guex & Peitsch, 1997 http://www.expasy.ch/spdbv/mainpage.html). The root-mean-square (RMS) deviation between the aligned structures is given for both side-chain atoms only, and for all atoms. CLP, cubic lipid phase; EM, electron diffraction with electron microscope.

(1) Grigorieff *et al*. (1996); (2) Pebay-Peyroula *et al*. (1997); (3) Kimura *et al*. (1997); (4) Mitsuoka *et al*. (1999); (5) Takeda *et al*. (1998); (6) Luecke *et al*. (1998); (7) Essen *et al*. (1998).

[a] Average for all three molecules in the asymmetric unit.

Retinal-binding pocket and the active site

In Figure 1(a) the electron density map defines the configuration of the all-*trans* retinal and its immediate surroundings. The polyene chain and the β-ionone ring are within 3.6 Å from the side-chains of Trp86, Thr89, Thr90, Met118, Trp138, Ser141, Thr142, Met145, Trp182, Tyr185, Trp189, and Asp212. Site-specific mutagenesis of many of these residues resulted in changed absorption maxima or changed rate of thermal isomerization (e.g. see Marti *et al*., 1991; Sonar *et al*., 1993; Ihara *et al*., 1994; Delaney *et al*., 1995; Weidlich *et al*., 1996). The side-chain of Leu93, a residue that was found to influence the rate of 13-*cis*-to all-*trans* reisomerization in the photocycle (Delaney *et al*., 1995), is as close as 3.6 Å from the 13-methyl group of the retinal. The angle between the retinal chain and the plane of the bilayer was determined to be 21° by polarized FTIR difference spectroscopy (Earnest *et al*., 1986), in excellent agreement with our structure where it is 20.5°. From linear dichroic measurements, the angle between the transition moments of the $N \rightarrow C_5$ and the $N \rightarrow H$ vectors was found to be 70° (Lin & Mathies, 1989). We find this angle to be 75°, i.e. nearly the same.

Bound water molecules near the Schiff base, Asp85, and Asp212 are shown in Figures 1(a) and 2. The presence of water in this region had been suggested earlier by the effects of mutations of these residues on the frequency shifts of O-H stretch bands during the photoreaction cycle (Maeda *et al*., 1994; Kandori *et al*., 1995; Hatanaka *et al*., 1997). The hydrogen-bonded network, which comprises the positively charged Schiff base, the three water molecules W401, W402, and W406, as well as Asp85 and Asp212 (Figures 1(a), 2 and 3), stabilizes the separated charges at the active site in the unphotolyzed state. Asp85 is kept anionic by additional hydrogen-bonding of its OD2 to the OH of Thr89, and Asp212 by hydrogen-bonding of its OD1 and OD2 to the phenolic OH of Tyr57 and Tyr185, respectively, as well as another hydrogen bond of OD1 to W406 that connects further to the positively charged Arg82. Disruption of the balanced geometry of this region upon all-*trans* to 13-*cis* photoisomerization of the retinal will destabilize the active site, and cause dissociation of the protonated Schiff base. The stabilization of the

Table 3. Interhelical main-chain to side-chain and side-chain to side-chain hydrogen bonds within monomers

Helices	Hydrogen-bonding partners
A - B	Arg7 (NH2) and Leu61 (O)
	Arg7 (NH2) and Met60 (O)
B - C	Thr46 (OG1) and Asp96 (OD2)
	Tyr57 (OH) and Arg82 (NH1) *via* water 407
C - D	Leu87 (O) and Asp115 (OD1) *via* water 511
	Thr90 (OG1) and Asp115 (OD1)
D - E	Met118 (O) and Ser141 (OG)
	Ala126 (O) and Arg134 (NH1)
	Thr128 (O) and Arg134 (NH1)
E - F	Trp138 (NE) and Pro186 (O)
	Arg134 (NE) and Glu194 (O)
	Arg134 (NH2) and Glu194 (O)
	Leu152 (O) and Arg175 (NH1)
F - G	Trp182 (NE) and Ala215 (O) *via* water 501
	Tyr185 (OH) and Asp212 (OD1)
	Ser193 (OG) and Glu204 (OE1)
	Ser193 (N) and Glu204 (OE1)
	Glu194 (OE1) and Glu204 (OE2)
G - A	Leu224 (O) and Lys30 (NZ)
A - C	Arg7 (NH1) and Tyr79 (OH)
	Glu9 (OE1) and Tyr79 (OH)
B - F	Tyr57 (OH) and Asp212 (OD2)
B - G	Ty57 (OH) and Thr205 (O) *via* water 407
C - F	Tyr79 (N) and Glu194 (OE1) *via* water 404
	Tyr83 (OH) and Trp189 (NE1)
C - G	Thr46 (O) and Lys216 (O) *via* water 502
	Tyr79 (O) and Glu204 (OE2) *via* water 405
	Arg82 (NH1) and Thr205 (O) *via* water 407
	Arg82 (NH2) and Thr205 (O) *via* water 407
	Asp85 (OD2) and Asp212 (OD1) *via* water 402
	Asp85 (OD2) and Lys216 (NZ) *via* water 402

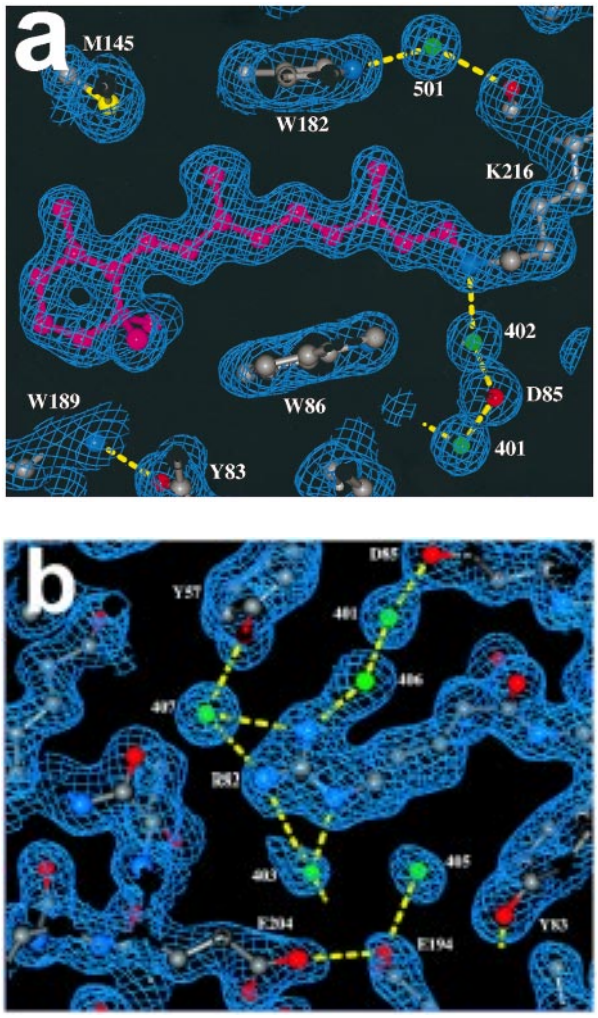

Figure 1. Electron density maps ($2F_o - F_c$) contoured at 1σ. (a) Region of the active site that contains an all-*trans* retinal. The plane of Trp86 and Trp182 flank the polyene chain between the 9-methyl and 13-methyl groups, and contribute to its immobilization in the retinal-binding pocket. Part of the hydrogen-bonded chain that leads from the Schiff base to the extracellular surface *via* water 402, Asp85, and water 401, is visible in this view. Water 501, which connects the peptide CO of Ala215 with the indole NH of Trp182, is also visible. The corresponding omit map with all retinal atoms omitted from the model still features a hole in the β-ionone ring, and can be viewed at http://anx12.bio.uci.edu/ ~ hudel/br/1.55/ret_omitmap.gif. (b) Region of Arg82 in the extracellular half channel. In the top portion, the guanidinium moiety is connected to the Schiff base *via* water 406, water 401, and Asp85 (see also Figures 2 and 3(b)). Water 407 further stabilizes the positive charge by accepting hydrogen bonds from both guanidinium nitrogen atoms. In the bottom portion, the connection to the extracellular surface continues *via* water 403, water 404 (not visible from this angle), Glu194 and Glu204. An omit map of this region, with all Arg82, Glu194 and Glu204 side-chain atoms and surrounding water molecules omitted from the model, can be viewed at http://anx12.bio.uci.edu/ ~ hudel/br/1.55/r82_omitmap.gif.

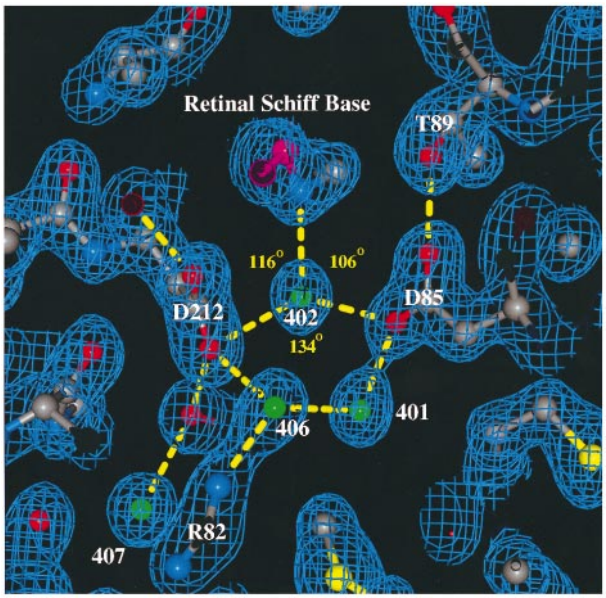

Figure 2. Electron density map ($2F_o - F_c$) of the region near the retinal Schiff base, contoured at 1σ. It shows the protonated Schiff base and water molecule 402, which is tightly hydrogen-bonded between the positively charged Schiff base and two negatively charged residues, the initial proton acceptor Asp85, and Asp212. The Schiff base nitrogen atom, water 402 and the two acceptor oxygen atoms of Asp85 and Asp212 lie in a plane. The angle between the two acceptor oxygen atoms with water 402 at the vertex is 134°. The angles between the Schiff base nitrogen atom and the oxygen of Asp85 and Asp212 with water 402 at the vertex are 106° and 116°, respectively. Also shown is water molecule 401, which connects Asp85 with Arg82 *via* water 406 (see also Figure 1(b)).

anionic form of Asp212 by hydrogen-bonding with the two sterically restricted tyrosine residues explains why Asp85, rather than Asp212, is the proton acceptor in this first and critical event in the transport. W402, which, *via* three strong hydrogen bonds, is centered between three formally charged moieties (Figure 2), may participate actively in this step. It is in a position where its dissociation to H^+ and OH^- could be part of the protonation/deprotonation events at the early stage of the transport cycle.

The extracellular region

As shown in Figures 1(b) and 2, and schematically in Figure 3, the Schiff base is connected to Arg82 and to the extracellular surface by an extensive three-dimensional hydrogen-bonded network. The participants in this network were identified in the earlier 2.3 Å map (Luecke *et al.*, 1998), but at 1.55 Å resolution four additional ordered water molecules, W404, W405, W406 and W407, become evident. The Schiff base is linked to Arg82 by a

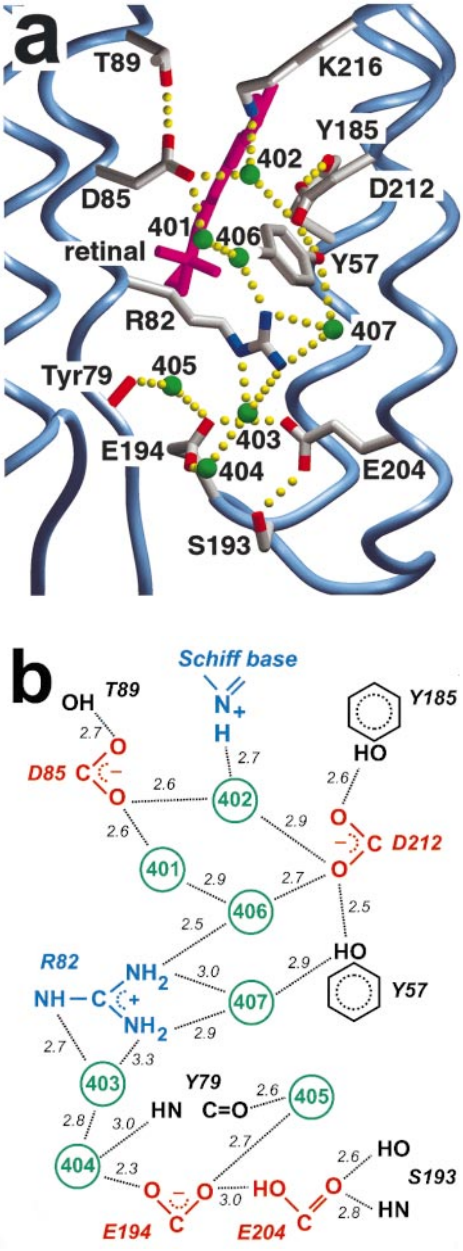

Figure 3. Extracellular region of bacteriorhodopsin. (a) View from the direction of helix C. The region of Ser193 is the F-G interhelical loop at the extracellular membrane surface. Hydrogen bonds visible from this angle are drawn as broken yellow lines. The retinal is purple; water molecules are green. (b) A representation of the hydrogen-bond network from the retinal Schiff base to the extracellular surface. Glu194 is shown unprotonated, because in the E194D mutant the pK_a of residue 194 is 3 (Dioumaev *et al.*, 1998). Glu204 is assumed to be protonated because it would be unstable as an anion if Glu194 were negatively charged.

continuous hydrogen-bonded chain comprising W402 - Asp85-OD1 - W401 - W406 - Arg82-NH2. A second chain, comprising W402 - Asp212-OD1 - Tyr57-OH - W407, leads to Arg82-NH1/NH2. This interconnected branched network of six residues, four water molecules, and 11 hydrogen bonds must constitute the diffuse negative counterion to the Schiff base suggested earlier from NMR spectroscopy (De Groot *et al.*, 1989), as it provides the means to delocalize the charges of Asp85 and Asp212.

Earlier, the region around Arg82 had been difficult to refine because its density was either missing (Henderson *et al.*, 1990; Grigorieff *et al.*, 1996) or ambiguous. In some structural models the side-chain of this residue points toward the Schiff base (Kimura *et al.*, 1997; Pebay-Peyroula *et al.*, 1997; Luecke *et al.*, 1998) while in others toward the extracellular surface (Henderson *et al.*, 1990; Grigorieff *et al.*, 1996). At the resolution now available, Arg82 is unambiguously in a conformation between these two (Figures 1(a) and 3(a)), in a position similar to that reported by Essen *et al.*, (1998). However, the electron densities of the side-chains of Glu194, Glu204, as well as W403, are less well defined than the densities of the residues that surround them. The structure we show for this region is the predominant one, but the density map is best interpreted with some degree of conformational heterogeneity. In omit maps, where Arg82, Glu194, Glu204 and the nearby water molecules are all left out of the model, the density for Glu204 suggests that in addition to the modeled structure there is a second conformation, in which the side-chain of this residue is closer to the guanidinium group of Arg82. The existence of a second, minor conformation is suggested also by the fact that the densities for Glu194 and W403 are less well defined than their surroundings. In this second conformation, Glu194 is hydrogen-bonded to the OH of Tyr83, and W403 is closer to NH1 of Arg82.

In the orientation of Arg82 in Figures 1(b) and 3, its side-chain is connected to Asp85, and accounts for the observation that the pK_a of Asp85 is increased by 4.5 pH units in the R82Q and R82A mutants (Otto *et al.*, 1990; Brown *et al.*, 1993). Arg82 is connected to the extracellular membrane surface by a linear network comprising W403 - W404 - Glu194-OE1 - Glu194-OE2 - Glu204-OE1 - Glu204-OE2 - Ser193-OH, stabilized additionally by water molecule W405. The water molecules W404 and W405 are stabilized by hydrogen-bonding with the peptide NH and C=O groups of Tyr79.

The anomalous titration of Asp85, which revealed two apparent pK_a values for this residue, has been suggested to reflect the influence of the proton occupancy of the extracellular proton release site on the proton occupancy of Asp85 (Balashov *et al.*, 1996). This coupling is the likely origin of the proton release upon protonation of Asp85 and the rise of the pK_a of Asp85 upon proton release in the photoreaction cycle (Balashov *et al.*, 1996; Richter *et al.*, 1996; Dioumaev *et al.*, 1998). Indeed, site-specific mutation of Arg82, Glu204, or Glu194 removes the coupling between Asp85 and the proton release site, and there is no

proton release in the cycle when Asp85 becomes protonated. The hydrogen-bonded network in Figure 3 provides the structural rationale for the required electrostatic coupling. However, the origin of the released proton is still uncertain. When Glu194 is changed to an aspartate residue, it has a pK_a of 3, and during the photocycle becomes transiently protonated consistent with a proton conducting, rather than proton donating, role for this residue (Dioumaev *et al*., 1998). Infrared spectra do not reveal the negative C═O stretch band from Glu204 expected if this residue were the proton release site (Rammelsberg *et al*., 1998). From the 2.3 Å resolution structure, we had suggested (Luecke *et al*., 1998) that the proton might originate from a water molecule hydrogen-bonded to Arg82. Another possibility is that the release is from a hydrogen-bonded continuum of water molecules in which a proton is delocalized (Rammelsberg *et al*., 1998). A third suggestion (Essen *et al*., 1998) is that the proton released is one shared by Glu194 and Glu204. The structure of the unphotolyzed state does not discriminate among these alternatives.

The proton release complex is well insulated from the aqueous medium. The region that contains water molecules W403, W404, W405, together with Glu194 and Glu204, is shielded from the extracellular aqueous interface by Ile78 and Leu201. At the C-terminal end of helix D a buried, an unpaired arginine residue (Arg134) is located near Glu194. A salt-bridge between these residues was suggested earlier (Grigorieff *et al*., 1996). While the positively charged guanidinium group of Arg134 interacts closely with three peptide carbonyl groups, from residues 126, 128, and 194, it is >5 Å from the closest side-chain carboxyl of Glu194, in agreement with the 2.9 Å model presented by Essen *et al*., (1998). This region is shielded from the bulk solvent by the aromatic side-chain of Phe71.

A π-bulge-induced kink at the middle of helix G

On the cytoplasmic side, the electron density map reveals that transmembrane helix G contains the kink reported in a recent model (Mitsuoka *et al*., 1999), and we find that it results from a π-bulge at residue 215 (Figure 4). This causes the peptide plane between Ala215 and Lys216 to tilt away from the helix axis, and locally disrupts the α-helical hydrogen-bonding pattern. Thus, the carbonyl group of residue 213 forms a hydrogen bond with the amide group of residue 218, and the carbonyl group of residue 214 interacts with the amide group of residue 219. The peptide carbonyl group of Ala215 does not participate in backbone hydrogen-bonding but accepts a hydrogen bond from water molecule W501 (Figure 5(a) and (b)). W501 in turn forms a hydrogen bond with the indole nitrogen atom of Trp182, a residue in van der Waals contact with the polyene chain of the retinal (Figure 1(a)). The α-helical structure of helix G resumes on the cytoplasmic side of the π-bulge, but in a direction about 15° tilted away from the center (Figure 5(c)). This results in outward displacement of the C-terminal portion of helix G (residues 222-225) by nearly one helix diameter when compared to a model α-helix aligned with the N-terminal portion of helix G. The novel non-proline kink in helix G is illustrated in more detail in Figure 6, which shows RMS deviations of main-chain atoms of the seven helices in the structure from those in aligned perfect helices. The deviations in helices B, C and F are associated with intramembrane proline residues, Pro50, Pro91, and Pro186, as expected. The sharp deviation in helix G, however, is located where there is no proline residue, and must be the result of the π-bulge shown in Figures 4 and 5.

Such π-bulges within α-helices are observed infrequently (Keefe *et al*., 1993), and appear to play mostly structural rather than directly functional roles. However, molecular dynamics simulation of an α-helix → π-bulge transition of a transmembrane protein (Duneau *et al*., 1996) suggested that the resulting redistribution of residues along the helical faces might have a functional role. Indeed, helix G does undergo a conformational change,

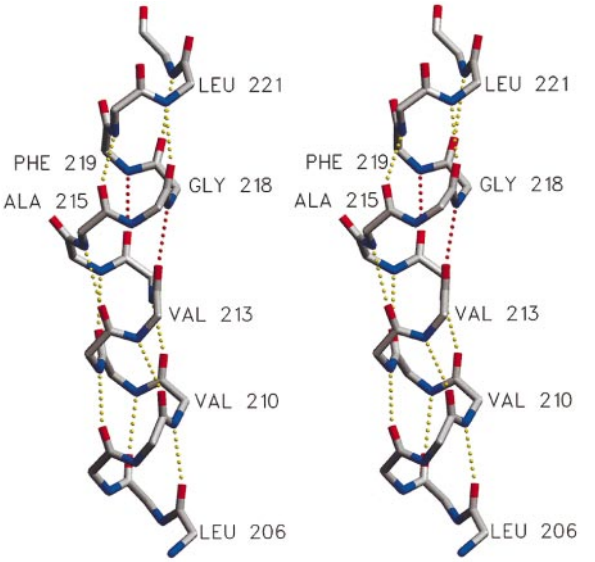

Figure 4. Stereo diagram of the π-bulge and kink in helix G. The π-bulge at Ala215 causes the peptide plane between Ala215 and Lys216 to tilt away from the helix axis, locally disrupting the α-helical hydrogen-bonding pattern. Thus, the carbonyl group of residue 213 hydrogen bonds with the amide of residue 218, and the carbonyl group of residue 214 interacts with the amide group of residue 219. The π-helical ($n \rightarrow n+5$) hydrogen bonds are shown in red, the α-helical ($n \rightarrow n+4$) hydrogen bonds in yellow. The disruption is local, with regular α-helical conformation on both sides of the bulge. The carbonyl group of Ala215 does not participate in backbone hydrogen-bonding.

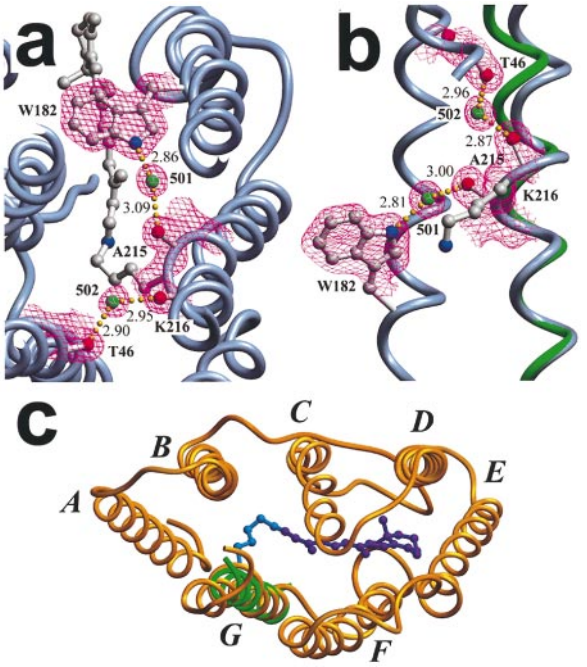

Figure 5. The π-bulge-induced kink of helix G. (a) View perpendicular to the bilayer plane, from the cytoplasmic side. Water molecule W501 forms a bridge between helices F and G, positioned 2.9 Å from the carbonyl group of Ala215, and 3.1 Å from the indole nitrogen atom of Trp182 with a *B* factor of 21 Å^2. Water molecule W502 forms a bridge between helices B and G, positioned 3.0 Å from the carbonyl group of Lys216, and 2.9 Å from the carbonyl group of Thr42 with a *B* factor of 31 Å^2. The retinal is also shown, in its binding cleft. Electron density ($2F_o - F_c$) is contoured at 1σ. (b) View parallel with the bilayer plane, showing the origin of the kink of helix G. The actual helix trace is colored gray; a model α-helix aligned with the extracellular half of helix G (residues 201-211) is colored green. (c) View of the whole monomer perpendicular to the bilayer plane, from the cytoplasmic side, showing direction and magnitude of the kink of helix G. The actual backbone trace is colored yellow; a model α-helix aligned with the first half of helix G (residues 201-211) is colored green. The kink results in the outward displacement by nearly one helix diameter of the C-terminal portion of helix G.

although so far poorly defined, during the bacteriorhodopsin photocycle (Dencher *et al*., 1989; Subramaniam *et al*., 1993; Han *et al*., 1994; Vonck, 1996; Kamikubo *et al*., 1996, 1997).

Further stabilization of this disrupted region is provided by a second water molecule, W502, which bridges the carbonyl group of the residue to which the retinal is attached *via* a Schiff base linkage, Lys216, to the carbonyl group of Thr46 of helix B (Figures 5(a) and (b)). The Schiff base and the carboxyl side-chain of Asp96 are 11 Å apart, necessitating some means for proton transfer when the Schiff base is reprotonated by Asp96 during the photocycle. Water 502 is located between the Schiff base and Asp96, 5.0 Å from Asp96, and 7.8 Å from the Schiff base in the all-*trans* retinal conformation, making it a prime candidate for participation in this proton conduction.

Through the hydrogen bonds at the π-bulge, which form the chains Ala215-O - W501 - Trp182-NE and Lys216-O - W502 - Thr46-O, helix G is linked to functionally important regions of the protein, i.e. to the C_{13}═C_{14} double bond of the retinal chain (*via* its contact with Trp182 through the C_{13} methyl group) and Asp96 (*via* its hydrogen bond with Thr46-OH). Thus, the structure provides the means for mutual interaction of the conformation of the main chain of helix G with the isomeric state of the retinal and the protonation state of Asp96. Asp96 has a high pK_a, maintained by the hydrophobic residues Ile45, Leu223, and Leu224 that form the sides of a barrel around it, with lids provided by Phe42, Leu99, and Leu100 from the cytoplasmic side, and by Val49, Leu93, and Phe219 from the direction of the retinal Schiff base. Rearrangements of the main chain in helix G and water molecules in this region may contribute to the required lowering of the pK_a of Asp96 during its function as a proton donor in the photochemical cycle (Cao *et al*., 1993), as well as mediate the observed coupling of the subsequent reprotonation of Asp96 from the bulk with the thermal reisomerization of the retinal to all-*trans*.

Structure of the lipid matrix in the crystals

Bacteriorhodopsin in the purple membrane is in intimate interaction with specific lipids that influence the thermal steps of the photochemical cycle (Joshi *et al*., 1998). According to previous analysis, purple membranes contain five distinct lipids: approximately five phosphatidyl glycerophosphate (methyl ester), 2 glycolipid sulfate, 0.5 phosphatidyl glycerol, and 0.5 phosphatidyl glycerosulfate, all containing dihydrophytyl chains, as well as one squalene (SQU) molecule per bacteriorhodopsin monomer (e.g. see Kates *et al*., 1982; Dracheva *et al*., 1996). Previous studies have provided some information on bacteriorhodopsin-lipid interaction in two-dimensional and three-dimensional crystals (Grigorieff *et al*., 1996; Essen *et al*., 1998; Takeda *et al*., 1998; Mitsuoka *et al*., 1999). During refinement of the present model, we noted numerous well-defined difference density features in the form of long narrow cylinders oriented parallel with the crystallographic *c*-axis. From these features, we identified 18 lipid chains. Four of these are shorter than full-length because of lack of interpretable electron density. Four individual pairs of full-length chains could be linked with a glycerol backbone, thereby identifying four diether lipids. Lipid head-group densities were observed in many instances but we did not model them because of their lower quality and ambiguity. The fact that we

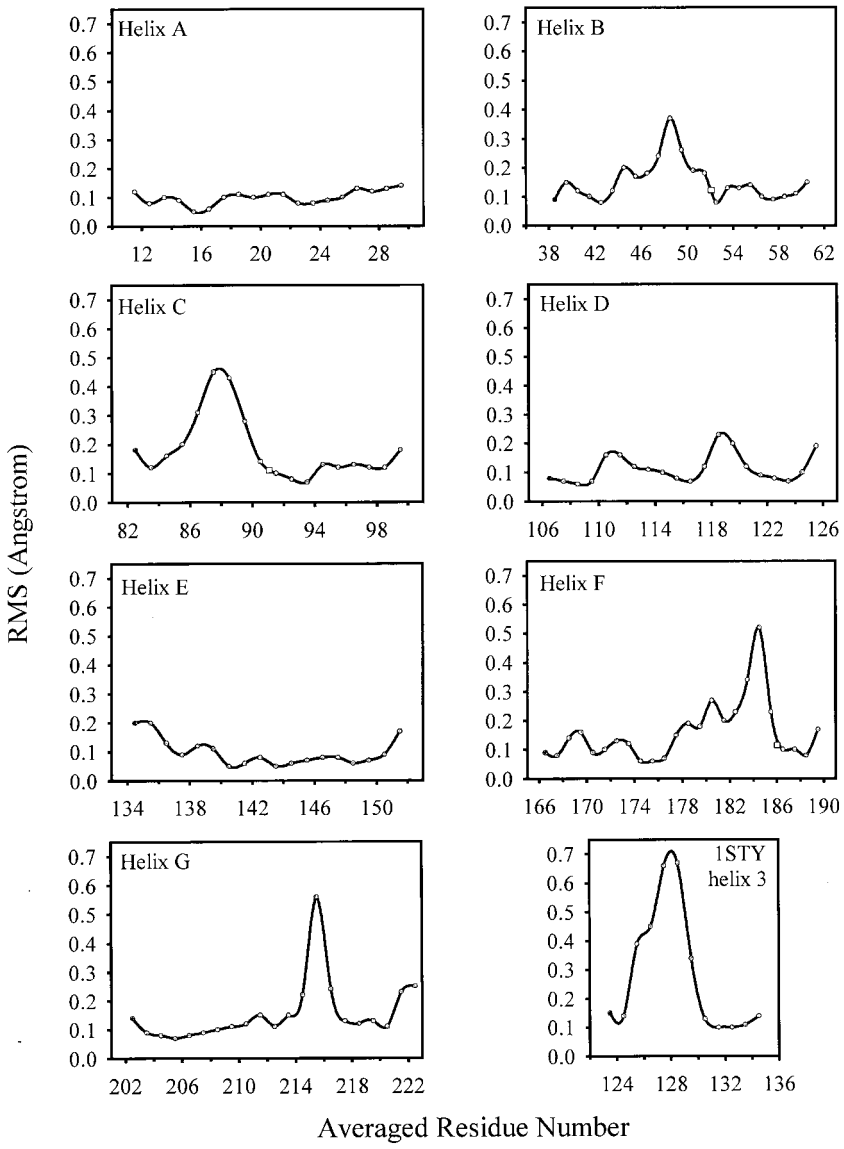

Figure 6. Root-mean-square (RMS) deviations of the seven bacteriorhodopsin helices from an idealized four-turn alpha helix ($\phi = -57^{o}$ and $\phi = -47^{o}$), calculated using Swiss-PDB-Viewer. The resulting plots illustrate the deviations from a regular alpha helix. Helices A, D, and E do not show consistent deviations from a perfect alpha helix. Helices B, C, and F exhibit deviations at specific locations due to proline-induced kinks of the main chain (Pro50, Pro91, and Pro186, marked as open squares). Consistent with the interpretation of the structural model in Figures 4 and 5, helix G has a sharp kink near Lys216 that is not associated with a proline residue. Also shown is a plot for an insertion mutant of staphylococcal nuclease (PDB code 1STY), which has a well-described π-bulge-induced kink due to a glycine insertion between residues 126 and 127 (Keefe *et al.*, 1993). The main-chain carbonyl group at this π-bulge, which does not participate in intra-helical hydrogen-bonding, is stabilized by a water molecule in a manner similar to the stabilization of the CO of Ala215 by W501 in bacteriorhodopsin.

observe diether lipids, and could model numerous phytanyl methyl groups, indicates that native purple membrane lipids were carried along through the detergent extraction of bacteriorhodopsin, since only monoacyl and unbranched lipid (mono-olein), is used in preparing the lipid cubic phase (Landau & Rosenbusch, 1996).

The lipids form a bilayer in the spaces between adjoining monomers and trimers (Figure 7). Nearly all space between the monomers in the *a/b* plane is taken up by ordered lipids. The average *B* factor for lipid atoms is 57 Å^2, as compared to 26 Å^2 for protein atoms (Table 1), reflecting their higher thermal motion. Since lipid bilayers are naturally fluid systems, their thermal disorder is likely to be higher than that of the associated protein even when restricted by the crystal lattice. The bilayer center is occasionally crossed by a few carbon atoms of a

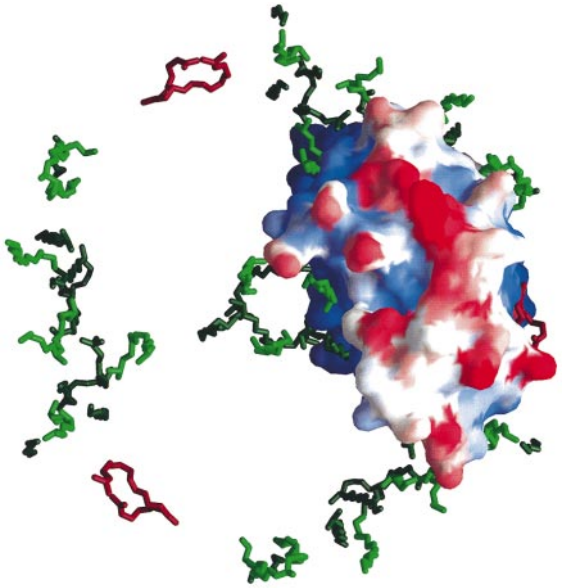

Figure 7. View of a trimer perpendicular to the bilayer plane, with one of the three proteins and all ordered lipid chains shown. Saturated palmityl (C-16) chains were used during initial lipid model building. Lipids atoms were modeled into continuous electron densities at contouring levels of 2.0 σ in the $F_o - F_c$, and 0.8 σ in the $3F_o - 2F_c$ maps. Where density was present, the chains were subsequently linked with a glycerol moiety to form diether lipids. The central region around the 3-fold axis is occupied by six diether lipid molecules. The remaining lipids form an annulus around the trimer, and are primarily responsible for crystal contacts in the plane of the bilayer. The protein surface is colored according to refined temperature factors (blue lower, red higher).

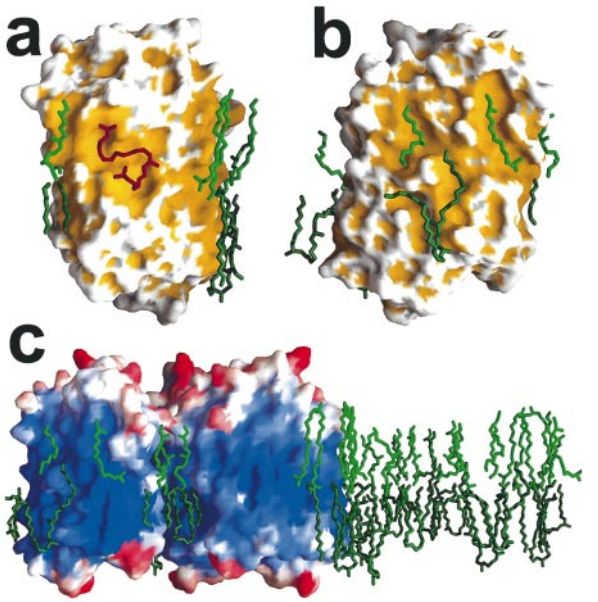

Figure 8. Side-view of the protein and ordered lipids. The protein surface is colored according to surface curvature, demonstrating the complementarity between the concave protein surface and the ordered lipids. (a) The S-shaped lipid molecule colored red is located near the center of the bilayer. This object is tentatively modeled as squalene. (b) Orientation (a) rotated about 90° around the vertical axis. The alkyl chains of a diether lipid are splayed apart by a bump in the protein surface. (c) The protein surface is colored according to refined temperature factors (blue lower, red higher). The ordered lipid tails (green) are arranged in a bilayer. The extracellular portion of the protein (bottom) is more completely embedded in the hydrophobic bilayer than the cytoplasmic region (top).

monolayer lipid that overlap into the other monolayer (Figure 8(c)). The center of the bilayer is offset by 5 Å from the center of the bacteriorhodopsin molecule toward the extracellular side. As a result, the cytoplasmic part of the protein is considerably less buried in lipids than the extracellular part and consequently shows higher *B* factors. This may be relevant to the fact that the cytoplasmic portion, but not the extracellular portion, of the protein undergoes large-scale conformational change during the photochemical cycle (Subramaniam *et al.*, 1993; Vonck, 1996). Similar conformational changes, described as rigid-body motions of the same transmembrane helices as in bacteriorhodopsin, have been detected by spin-spin distance measurements also in visual rhodopsin (Farrens *et al.*, 1996).

The compact arrangement in the *a*/*b* crystallographic plane, which is equivalent to the biologically relevant purple membrane sheets that also form a p3 lattice with $a = b = 61$ Å (Table 1), warrants further analysis. Upon trimer formation, 13.9 % (1376 Å^2) of the monomer accessible surface area (Nicholls *et al.*, 1991) is buried. The trimer, with an equal buried fraction, loses an additional 1.2 % (310 Å^2) when embedded within symmetry-related trimers, demonstrating minimal direct contact between the individual trimers in the bilayer plane. This implies that crystal contacts in the bilayer plane are mediated almost exclusively by lipid molecules that fill the cavities between the molecules. An additional 39.6 % (10,194 Å^2) of the trimer surface area is excluded by this lipid bilayer (Figures 7 and 8(c)). Overall, 54.7 % (14,632 Å^2) of the trimer is buried by a combination of protein-protein and protein-lipid interactions. The center of the trimer contains two lipids (LIP608 and LIP618) per monomer (Figure 7), which cover 8.1 % (2073 Å^2) of the trimer surface. The remaining lipids form an annulus around the external surface of the trimer.

Most of the lipid chains are only slightly bent or curved, but one (SQU701) adopts an S-shape (Figure 8(a)) clearly evident in the electron density maps prior to lipid model building. This feature is located within the core of the bilayer, and is tightly

associated with the protein surface where a complementary groove, formed by the side-chains of Leu19, Leu22, Val210, Val213, Val217, Leu221, as well as by the side-chain of Ser214 hydrogen-bonded to the peptide C═O of Val210, exists near the π-bulge of helix G. Squalene is present in purple membranes, in equimolar amount to bacteriorhodopsin. We have modeled this feature tentatively as squalene. Its location at the distorted, and presumed functionally active, region of helix G would be consistent with the observation that squalene strongly affects reprotonation of the retinal Schiff base by Asp96 during the photocycle (Joshi *et al.*, 1998). The presence of squalene, as well as the other native lipids, is suggested also by the fact that the photochemical cycle is essentially the same in these crystals as in the bacteriorhodopsin-containing membranes before their solubilization (Luecke *et al.*, 1998; Heberle *et al.*, 1998).

Accessible surface plots of bacteriorhodopsin, colored and shaded according to surface curvature and *B* factor, respectively, are shown in Figures 8(a) and (b). The part of the protein that is buried in the bilayer is more compact and rigid than the solvent-exposed part. On the hydrophobic protein surface, grooves are formed by specific arrangements of the side-chains. The highly structured lipid-protein interface provides clues to the forces that stabilize the boundary lipids around this membrane protein. Whether they are straight or bent, the lipid chains are aligned with these grooves throughout, and imply specific interactions between the lipid chains and the protein groups. Theoretical models have predicted the existence of such intimate lipid-protein contacts, and that the interaction would be based on van der Waals - London forces (White & Wimley, 1999). We now report direct evidence for this in the bacteriorhodopsin structure.

Conclusions

At 1.55 Å resolution it is evident that bacteriorhodopsin contains a continuous hydrogen-bonded chain of residues and bound water molecules on the extracellular side of the centrally located retinal Schiff base, and a discontinuous chain on the cytoplasmic side. This arrangement provides both for the coupling of proton release upon deprotonation of the Schiff base, and for a barrier to proton conduction in the unphotolyzed protein. The proton release to the extracellular surface, which occurs early in the photochemical cycle, will utilize the interactions in the preformed extracellular hydrogen-bonded network. Proton transfer from the cytoplasmic surface to the active site, which is delayed until later in the cycle, will depend, however, on forming a network not present in the unphotolyzed structure. The observed non-proline kink of helix G through hydrogen-bonding of two water molecules provides a structural rationale for how the large-scale conformational change in the cytoplasmic region could establish a transient proton conduction pathway.

The lipid bilayer in which the individual bacteriorhodopsin trimers are embedded is in direct contact with more than 80 % of the protein surface. The protein surface provides pronounced grooves with which the lipid tails interact, displaying a surprising extent of structural complementarity. Similar features are likely to play important roles in the interaction of many membrane proteins with their native lipids.

Materials and Methods

Data collection

Crystals were grown as described (Landau & Rosenbusch, 1996), and form thin hexagonal plates of typically about 80 μm × 80 μm × 15 μm. After mechanical extraction of the crystals, the adhering cubic lipid phase was removed by soaking for several hours in 0.1 % (w/v) octylglucoside solution containing 3 M sodium phosphate at pH 5.6. Diffraction data were collected from a single light-adapted, cryo-cooled (100 K) crystal at beamline 5.0.2 at the ALS (Lawrence Berkeley Lab.) synchrotron using a 2 × 2 array CCD detector (ADSC, San Diego): 100 images of 1° in ϕ with a 60 second exposure time were integrated, scaled and merged with DENZO/SCALEPACK (Otwinowski, 1993). The space group is $P6_3$ with $a = b = 60.6$ Å and $c = 108.2$ Å.

Refinement

The starting model (1BRX, Luecke *et al.*, 1998) was refined with SHELXL-97 (Sheldrick & Schneider, 1997) taking partial merohedral twinning into account. Omit maps and $3F_o - 2F_c$ maps were employed extensively in refitting side-chain conformations, locating extra water molecules and fitting lipid tails. The final model includes residues 5-156, 162-231, the covalently linked retinal, 24 water molecules and 14 lipid molecules. The N and C termini, as well as the E-F loop between residues 156 and 162, are too disordered to allow interpretation. The Ramachandran plot places 97.9 % of all residues in the core region, and 2.1 % in the allowed region.

Secondary structure

Secondary structure assignments were made after careful consideration of hydrogen-bonding geometries. Hydrogen-bonding required a NH···O distance of 2.3 Å or shorter and an angle (N, H, O) of 120° or more. Alpha helices: A, residues 9-31; B, residues 36-63; C, residues 81-101; D, residues 104-127; E, residues 133-155 +; F, residues 164-192; G, residues 200 to 225, with the exception of the π-bulge around residue 215. Beta strands: BC(I), residues 67-71; BC(II), residues 74-78.

Protein Data Bank access codes

The coordinates of the structure and the SHELXL-detwinned structure factors for map calculations have been

deposited in the Protein Data Bank (entry code 1C3W), and are available at *http://anx12.bio.uci.edu/~hudel/br/1.55/1c3w.pdb* and/*1c3w.fob*, respectively.

Acknowledgements

We thank the beamline staff at the Advanced Light Source (ALS) in Berkeley and at the Stanford Synchrotron Radiation Laboratory (SSRL) for their continuing support. We are also grateful to Stephen White, Robert Glaeser and Ara Apkarian for discussion and encouragement. This work was supported, in part, by grants from the NIH to H.L. (R01-GM56445) and J.K.L. (R01-GM29498), and from the DOE to J.K.L. (DEFG03-86ER13525).

References

Balashov, S. P., Imasheva, E. S., Govindjee, R. & Ebrey, T. G. (1996). Titration of aspartate-85 in bacteriorhodopsin: what it says about chromophore isomerization and proton release. *Biophys. J.* **70**, 473-481.

Brown, L. S., Bonet, L., Needleman, R. & Lanyi, J. K. (1993). Estimated acid dissociation constants of the Schiff base, Asp-85 and Arg-82 during the bacteriorhodopsin photocycle. *Biophys. J.* **65**, 124-130.

Brown, L. S., Váró, G., Needleman, R. & Lanyi, J. K. (1995). Functional significance of a protein conformation change at the cytoplasmic end of helix F during the bacteriorhodopsin photocycle. *Biophys. J.* **69**, 2103-2111.

Cao, Y., Váró, G., Chang, M., Ni, B., Needleman, R. & Lanyi, J. K. (1991). Water is required for proton transfer from aspartate 96 to the bacteriorhodopsin Schiff base. *Biochemistry,* **30**, 10972-10979.

Cao, Y., Váró, G., Klinger, A. L., Czajkowsky, D. M., Braiman, M. S., Needleman, R. & Lanyi, J. K. (1993). Proton transfer from Asp-96 to the bacteriorhodopsin Schiff base is caused by decrease of the pK_a of Asp-96 which follows a protein backbone conformation change. *Biochemistry,* **32**, 1981-1990.

De Groot, H. J. M., Harbison, G. S., Herzfeld, J. & Griffin, R. G. (1989). Nuclear magnetic resonance study of the Schiff base in bacteriorhodopsin: counterion effects on the ^{15}N shift anisotropy. *Biochemistry,* **28**, 3346-3353.

Delaney, J. K., Schweiger, U. & Subramaniam, S. (1995). Molecular mechanism of protein-retinal coupling in bacteriorhodopsin. *Proc. Natl Acad. Sci. USA,* **92**, 11120-11124.

Dencher, N. A. & Heyn, M. P. (1979). Bacteriorhodopsin monomers pump protons. *FEBS Letters,* **108**, 307-310.

Dencher, N. A., Dresselhaus, D., Zaccai, G. & Büldt, G. (1989). Structural changes in bacteriorhodopsin during proton translocation revealed by neutron diffraction. *Proc. Natl Acad. Sci. USA,* **86**, 7876-7879.

Dioumaev, A. K., Richter, H. T., Brown, L. S., Tanio, M., Tuzi, S., Saitô, H., Kimura, Y., Needleman, R. & Lanyi, J. K. (1998). Existence of a proton transfer chain in bacteriorhodopsin: participation of Glu-194 in the release of protons to the extracellular surface. *Biochemistry,* **37**, 2496-2506.

Dracheva, S., Bose, S. & Hendler, R. W. (1996). Chemical and functional studies on the importance of purple membrane lipids in bacteriorhodopsin photocycle behavior. *FEBS Letters,* **382**, 209-212.

Duneau, J. P., Genest, D. & Genest, M. (1996). Detailed description of an alpha helix → pi bulge transition detected by molecular dynamics simulations of the p185c-erbB2 V659G transmembrane domain. *J. Biomol. Struc. Dynam.* **13**, 753-769.

Earnest, T. N., Roepe, P., Braiman, M. S., Gillespie, J. & Rothschild, K. J. (1986). Orientation of bacteriorhodopsin chromophore probed by polarized Fourier transform infrared difference spectroscopy. *Biochemistry,* **25**, 7793-7798.

Essen, L. O., Siegert, R., Lehmann, W. D. & Oesterhelt, D. (1998). Lipid patches in membrane protein oligomers: crystal structure of the bacteriorhodopsin-lipid complex. *Proc. Natl Acad. Sci. USA,* **95**, 11673-11678.

Farrens, D. L., Altenbach, C., Yang, K., Hubbell, W. L. & Khorana, H. G. (1996). Requirement of rigid-body motion of transmembrane helices for light activation of rhodopsin. *Science,* **274**, 768-770.

Grigorieff, N., Ceska, T. A., Downing, K. H., Baldwin, J. M. & Henderson, R. (1996). Electron-crystallographic refinement of the structure of bacteriorhodopsin. *J. Mol. Biol.* **259**, 393-421.

Han, B.-G., Vonck, J. & Glaeser, R. M. (1994). The bacteriorhodopsin photocycle: direct structural study of two substates of the M-intermediate. *Biophys. J.* **67**, 1179-1186.

Hatanaka, M., Kandori, H. & Maeda, A. (1997). Localization and orientation of functional water molecules in bacteriorhodopsin as revealed by polarized Fourier transform infrared spectroscopy. *Biophys. J.* **73**, 1001-1006.

Heberle, J., Büldt, G., Koglin, E., Rosenbusch, J. P. & Landau, E. M. (1998). Assessing the functionality of a membrane protein in a three-dimensional crystal. *J. Mol. Biol.* **281**, 587-592.

Henderson, R., Baldwin, J. M., Ceska, T. A., Zemlin, F., Beckmann, E. & Downing, K. H. (1990). Model for the structure of bacteriorhodopsin based on high-resolution electron cryo-microscopy. *J. Mol. Biol.* **213**, 899-929.

Hoff, W. D., Jung, K. H. & Spudich, J. L. (1997). Molecular mechanism of photosignaling by archaeal sensory rhodopsins. *Annu. Rev. Biophys. Biomol. Struct.* **26**, 223-258.

Ihara, K., Amemiya, T., Miyashita, Y. & Mukohata, Y. (1994). Met-145 is a key residue in the dark adaptation of bacteriorhodopsin homologs. *Biophys. J.* **67**, 1187-1191.

Iwata, S., Ostermeier, C., Ludwig, B. & Michel, H. (1995). Structure at 2. 8 Å resolution of cytochrome c oxidase from *Paracoccus denitrificans*. *Nature,* **376**, 660-669.

Iwata, S., Lee, J. W., Okada, K., Lee, J. K., Iwata, M., Rasmussen, B., Link, T. A., Ramaswamy, S. & Jap, B. K. (1998). Complete structure of the 11-subunit bovine mitochondrial cytochrome bc_1 complex. *Science,* **280**, 1934-1937.

Joshi, M. K., Dracheva, S., Mukhopadhyay, A. K., Bose, S. & Hendler, R. W. (1998). Importance of specific native lipids in controlling the photocycle of bacteriorhodopsin. *Biochemistry,* **37**, 14463-14470.

Kamikubo, H., Kataoka, M., Váró, G., Oka, T., Tokunaga, F., Needleman, R. & Lanyi, J. K. (1996). Structure of the N intermediate of bacteriorhodopsin revealed by X-ray diffraction. *Proc. Natl Acad. Sci. USA,* **93**, 1386-1390.

Kamikubo, H., Oka, T., Imamoto, Y., Tokunaga, F., Lanyi, J. K. & Kataoka, M. (1997). The last phase of the reprotonation switch in bacteriorhodopsin: the transition between the M-type and the N-type protein conformation depends on hydration. *Biochemistry,* **36**, 12282-12287.

Kandori, H., Yamazaki, Y., Sasaki, J., Needleman, R., Lanyi, J. K. & Maeda, A. (1995). Water-mediated proton transfer in proteins: an FTIR study of bacteriorhodopsin. *J. Am. Chem. Soc.* **117**, 2118-2119.

Kates, M., Kushwaha, S. C. & Sprott, G. D. (1982). Lipids of purple membrane from extreme halophiles and of methanogenic bacteria. *Methods Enzymol.* **88**, 98-111.

Keefe, L. J., Sondek, J., Shortle, D. & Lattman, E. E. (1993). The alpha aneurism: a structural motif revealed in an insertion mutant of staphylococcal nuclease. *Proc. Natl Acad. Sci. USA,* **90**, 3275-3279.

Kimura, Y., Vassylyev, D. G., Miyazawa, A., Kidera, A., Matsushima, M., Mitsuoka, K., Murata, K., Hirai, T. & Fujiyoshi, Y. (1997). Surface of bacteriorhodopsin revealed by high-resolution electron crystallography. *Nature,* **389**, 206-211.

Landau, E. M. & Rosenbusch, J. P. (1996). Lipidic cubic phases: a novel concept for the crystallization of membrane proteins. *Proc. Natl Acad. Sci. USA,* **93**, 14532-14535.

Lanyi, J. K. (1997). Mechanism of ion transport across membranes. Bacteriorhodopsin as a prototype for proton pumps. *J. Biol. Chem.* **272**, 31209-31212.

Lin, S. W. & Mathies, R. A. (1989). Orientation of the protonated retinal Schiff base group in bacteriorhodopsin from absorption linear dichroism. *Biophys. J.* **56**, 653-660.

Luecke, H., Richter, H. T. & Lanyi, J. K. (1998). Proton transfer pathways in bacteriorhodopsin at 2.3 Å resolution. *Science,* **280**, 1934-1937.

Maeda, A., Sasaki, J., Yamazaki, Y., Needleman, R. & Lanyi, J. K. (1994). Interaction of aspartate 85 with a water molecule and the protonated Schiff base in the L intermediate of bacteriorhodopsin: a Fourier transform infrared spectroscopy study. *Biochemistry,* **33**, 1713-1717.

Marti, T., Otto, H., Mogi, T., Rösselet, S. J., Heyn, M. P. & Khorana, H. G. (1991). Bacteriorhodopsin mutants containing single substitutions of serine or threonine residues are all active in proton translocation. *J. Biol. Chem.* **266**, 6919-6927.

Mitsuoka, K., Hirai, T., Murata, K., Miyazawa, A., Kidera, A., Kimura, Y. & Fujiyoshi, Y. (1999). The structure of bacteriorhodopsin at 3.0 Å resolution based on electron crystallography: implication of the charge distribution. *J. Mol. Biol.* **286**, 861-882.

Nicholls, A., Sharp, K. A. & Honig, B. (1991). Protein folding association: insights from the interfacial and thermodynamic properties of hydrocarbons. *Proteins: Struct. Funct. Genet.* **11**, 281-296.

Oesterhelt, D. (1998). The structure and mechanism of the family of retinal proteins from halophilic archaea. *Curr. Opin. Struct. Biol.* **8**, 489-500.

Otto, H., Marti, T., Holz, M., Mogi, T., Stern, L. J., Engel, F., Khorana, H. G. & Heyn, M. P. (1990). Substitution of amino acids Asp-85, Asp-212, and Arg-82 in bacteriorhodopsin affects the proton release phase of the pump and the p*K* of the Schiff base. *Proc. Natl Acad. Sci. USA,* **87**, 1018-1022.

Otwinowski, Z. (1993). SCALEPACK. In *Data Collection and Processing* (Sawyer, L., Isaacs, N. & Bailey, S., eds), pp. 56-62, SERC Daresbury Laboratory, Warrington, UK.

Pebay-Peyroula, E., Rummel, G., Rosenbusch, J. P. & Landau, E. M. (1997). X-ray structure of bacteriorhodopsin at 2.5 Å from microcrystals grown in lipidic cubic phases. *Science,* **277**, 676-1681.

Rammelsberg, R., Huhn, G., Lübben, M. & Gerwert, K. (1998). Bacteriorhodopsin's intramolecular proton-release pathway consists of a hydrogen-bonded network. *Biochemistry,* **37**, 5001-5009.

Richter, H. T., Brown, L. S., Needleman, R. & Lanyi, J. K. (1996). A linkage of the pK_a's of Asp-85 and Glu-204 forms part of the reprotonation switch of bacteriorhodopsin. *Biochemistry,* **35**, 4054-4062.

Sass, H. J., Schachowa, I. W., Rapp, G., Koch, M. H. J., Oesterhelt, D., Dencher, N. A. & Büldt, G. (1997). The tertiary structural changes in bacteriorhodopsin occur between M states; X-ray diffraction and Fourier transform infrared spectroscopy. *EMBO J.* **16**, 1484-1491.

Sheldrick, G. M. & Schneider, T. (1997). High resolution refinement. *Methods Enzymol.* **277**, 319-343.

Sonar, S., Krebs, M. P., Khorana, H. G. & Rothschild, K. J. (1993). Static and time-resolved absorption spectroscopy of the bacteriorhodopsin mutant Tyr-185 → Phe: evidence for an equilibrium between bR_{570} and an O-like species. *Biochemistry,* **32**, 2263-2271.

Spudich, J. L. (1994). Protein-protein interaction converts a proton pump into a sensory receptor. *Cell,* **79**, 747-750.

Spudich, E. N., Zhang, W. S., Alam, M. & Spudich, J. L. (1997). Constitutive signaling by the phototaxis receptor sensory rhodopsin II from disruption of its protonated Schiff base Asp-73 interhelical salt bridge. *Proc. Natl Acad. Sci. USA,* **94**, 4960-4965.

Subramaniam, S., Gerstein, M., Oesterhelt, D. & Henderson, R. (1993). Electron diffraction analysis of structural changes in the photocycle of bacteriorhodopsin. *EMBO J.* **12**, 1-8.

Takeda, K., Sato, H., Hino, T., Kono, M., Fukuda, K., Sakurai, I., Okada, T. & Kouyama, T. (1998). A novel three-dimensional crystal of bacteriorhodopsin obtained by successive fusion of the vesicular assemblies. *J. Mol. Biol.* **283**, 463-474.

Thorgeirsson, T. E., Xiao, W., Brown, L. S., Needleman, R., Lanyi, J. K. & Shin, Y.-K. (1997). Opening of the cytoplasmic proton channel in bacteriorhodopsin. *J. Mol. Biol.* **273**, 951-957.

Tsukihara, T., Aoyama, H., Yamashita, E., Tomizaki, T., Yamaguchi, H., Shinzawa-Itoh, K., Nakashima, R., Yaono, R. & Yoshikawa, S. (1996). The whole structure of the 13-subunit oxidized cytochrome *c* oxidase at 2.8 Å. *Science,* **272**, 1136-1144.

Váró, G., Needleman, R. & Lanyi, J. K. (1996). Protein structural change at the cytoplasmic surface as the cause of cooperativity in the bacteriorhodopsin photocycle. *Biophys. J.* **70**, 461-467.

Vonck, J. (1996). A three-dimensional difference map of the N intermediate in the bacteriorhodopsin photocycle: part of the F helix tilts in the M to N transition. *Biochemistry,* **35**, 5870-5878.

Weidlich, O., Schalt, B., Friedman, N., Sheves, M., Lanyi, J. K., Brown, L. S. & Siebert, F. (1996). Steric interaction between the 9-methyl group of the retinal and tryptophan 182 controls 13-*cis* to all-*trans* reisomerization and proton uptake in the

bacteriorhodopsin photocycle. *Biochemistry,* **35**, 10807-10814.

White, S. H. & Wimley, W. C. (1999). Membrane protein folding and stability: physical principles. *Annu. Rev. Biophys. Biomol. Struct.* **28**, 319-365.

Xia, D., Yu, C. A., Kim, H., Xia, J. Z., Kachurin, A. M., Zhang, L., Yu, L. & Deisenhofer, J. (1997). Crystal structure of the cytochrome bc_1 complex from bovine heart mitochondria. *Science,* **277**, 60-66.

Zhang, X. N., Zhu, J. Y. & Spudich, J. L. (1999). The specificity of interaction of archaeal transducers with their cognate sensory rhodopsins is determined by their transmembrane helices. *Proc. Natl Acad. Sci. USA,* **96**, 857-862.

Edited by D. C. Rees

(Received 17 May 1999; received in revised form 9 July 1999; accepted 11 July 1999)